High yield of H_2O_2 and efficient S recovery from toxic H_2S splitting through a self-driven photoelectrocatalytic system with a microporous GDE cathode

Li Qiao[a], Jing Bai[a,*], Tao Luo[a], Jinhua Li[a], Yan Zhang[a], Ligang Xia[a], Tingsheng Zhou[a], Qunjie Xu[b,c], Baoxue Zhou[a,c,d,*]

[a] School of Environmental Science and Engineering, Shanghai Jiao Tong University, No. 800 Dongchuan Rd., Shanghai, 200240, PR China
[b] College of Environmental and Chemical Engineering, Shanghai University of Electric Power, No.2588 Changyang Road, Shanghai, 200090, PR China
[c] Shanghai Institute of Pollution Control and Ecological Security, Shanghai, 200092, PR China
[d] Key Laboratory of Thin Film and Microfabrication Technology (Ministry of Education), Shanghai 200240, PR China

ABSTRACT

In this paper, the toxic H_2S was transformed efficiently into valuable S and H_2O_2 and its chemical reaction energy was converted into electric energy through a self-driven photoelectrocatalytic(PEC) system, which consisted of a microporous gas diffusion electrode(GDE) and a self-bias photoanode. In the cathode region, high yield of H_2O_2 up to 0.8 mmol/L/h, was achieved because of the fast gas diffusion and direct two-electron reduction of molecular oxygen on the microporous GDE cathode. In the anodic region, H_2S was completely converted into S without persulfide based on a I^-/I_3^- redox system and the production rate of S recovery was about 0.60 mmol/h, 42 times higher than before. The remarkable catalytic efficiency also benefited from the self-bias design of photoanode, which included a front photoanode of WO_3 and a rear Si photovoltaic cell (Si PVC). The constituted self-driven PEC system could accelerate the charges separation and increase the electron transfer rate of PEC cell. In addition, electricity was generated simultaneously, with a maximum power density of 0.19 mW/cm^2. The proposed self-driven PEC cell system offers an efficient, complete and sustainable way for H_2S resourcization.

1. Introduction

The industrialization of human society consumes large amount of limited fossil fuels and caused serious environmental problems, threatening the subsistence of all species living on the earth. Seeking efficient approaches to eliminating the pollutants has become a key issue of global concern and many efforts have been made to decompose the pollutants and clean the environment. However, many of pollutants are potentially valuable chemicals rich with energy. For instance, Hydrogen sulfide(H_2S) is a harmful and undesirable chemical [1–3], while H_2S is much favorable for dispose to recover elemental sulfur (S) as valuable resources [4]. However, the current processes such as Claus process, consume great amount of energy and will generate other contaminants (SOx).

In fact, photocatalytic [5–7] and photoelectrocatalytic (PEC) [8–13] techniques could be a sustainable and cost-effective technology to treat H_2S [14].

$$H_2S(aq) \rightarrow S\downarrow + H_2 \tag{1}$$

$\triangle G° = 33.0\,kJ.mol^{-1}$, $\triangle H° = 11.0\,kJ.mol^{-1}$

By introducing the cyclic redox I^-/I_3^- system [15,16], the H_2S can be conveniently and efficiently converted to S and H_2 [17,18]. However, this process was an endothermic reaction and need extra energy [Eq. (1)]. Besides, H_2 requires strict conditions for storage and usage. Comparably, direct conversion of H_2S into S and H_2O_2 is more favorable and therefore more easily implemented because this is a spontaneous process on thermodynamics [Eq. (2)]. Moreover, the product H_2O_2 is an important commodity oxidant [19,20]. How to realize the efficient productin of H_2O_2 became the key to complete the process.

$$H_2S(aq) + O_2 \rightarrow S\downarrow + H_2O_2(aq) \tag{2}$$

$\triangle G° = -106.2\,kJ.mol^{-1}$, $\triangle H° = -151.2\,kJ.mol^{-1}$

To yield H_2O_2, an anthra-quinone (AQ) process has been reported [18], in which hydrogenation of AQ with H produces anthrahydroquinone

(H_2AQ) and subsequent oxidation of H_2AQ by O_2 produces H_2O_2 [21]. However, the production rate of H_2O_2 was relatively low and the process needed extra addition of chemicals. Actually, the production of H_2O_2 depends on the reduction of molecular O_2 in the cathodic compartment. Pt, carbon felt and nickel foam are commonly used as cathodes to yield H_2O_2, but the output of H_2O_2 is far from enough. According to previous research, increasing the transfer rate of molecular O_2 and improving the direct two-electron reduction will help to yield H_2O_2 [22–24]. Based on this consideration, a specially designed gas diffusion electrode(GDE) was chosen as the cathode due to its microporous structure and high specific surface area which could help the diffusion of oxygen molecules to the surface of the cathode and the direct reduction of two-electron process.

On the other hand, how to accelerate the separation of photogenerated charges and increase the electron transfer rate in PEC process is still a key issue. In this study, we also constructed a self-driven PEC cell which consisted of the microporous GDE cathode and a self-bias photoanode to achieve the above objective. Under illumination, the self-driven photoanode could form a self-bias function by its front WO_3 and rear Si photovoltaic cell (Si PVC) [25], in which WO_3 mainly absorbs short-wavelength part of sunlight and generates electron/hole pairs [26–28]. Meanwhile, the filtered long-wavelength light can be captured by rear Si PVC to generate photovoltage [26], which will highly promote the separation of photogenerated charges and electron transfer rate of PEC cell.

In a word, we proposed a self-driven PEC system to decompose toxic H_2S, recover valuable S and H_2O_2 and generate electricity simultaneously. This newly designed system achieved remarkable catalytic efficiency, in which the yield of H_2O_2, up to 0.8 mmol/L/h, was nearly dozen times as previous report [18], and the production rate of S was remarkably enhanced as well.

2. Experimental

Unless otherwise indicated, all the chemicals used in this work were purchased from Sinopharm Group CO. LTD and were of analytical reagent. All solutions were prepared to use high-purity DI water.

2.1. Preparation of self-bias photoanode

The self-bias photoanode consisted of a front photoanode of WO_3 and a rear photocathode of Si photovoltaic cell (Si PVC). The effective area of the photoanode was 6 cm^2.

The WO_3 nano-flake arrays (NFA) was prepared through hydrothermal method [29]. In a typical process, 1 g of ammonium metatungstate{$(NH_4)_{10}(H_2W_{12}O_{42})$ ■$4H_2O$} was dissolved in 95 mL deionized water and stirred for 1 h. 2 mL of concentrated HCl (37%) was added and stirred for 1 h. Finally, 4 mL of H_2O_2(30%) was added and stirred for another 1 h to dissolve the tungstic acid. The WO_3 precursor solution was transferred to a Teflon reactor and the FTO substrate (Sigma-Aldrich, surface resistivity 7.3 Ω cm^{-1}, 2.5 × 4.5 cm^2) was diagonally placed in the reactor. The reactor was then put into the oven and the hydrothermal synthesis was conducted at 160℃ for 4 h. After the reactor cooled to the room temperature, the sample was taken out and flushed slightly with DI water. Finally, the sample was calcined in a muffle furnace at 500℃ for 2 h with a heating rate of 1℃/min.

The self-bias photoanode composed of a WO_3 NFA electrode, as the front photoanode and a commercial tetra-cell Si cell, as the rear PVC (Figure S1). The two electrodes were connected in series and were sealed by epoxy resin.

2.2. The preparation of GDE cathode

Figure S2 shows the fabrication process of GDE. Typically, 2.5 g prepared graphite powder, 0.25 g Na_2SO_4, 0.2 g acetylene black and 12.5 mL absolute ethyl alcohol were mixed and shaked in the ultrasonic

machine for 15 min. Then 0.833 g Polytetrafluoroethylene (PTFE) was added into the mixture at 80℃ until a paste was formed.

Due to its microporous structure and high specific surface area helps the rapid diffusion of oxygen molecules to the surface of the cathode and the direct reduction of two-electron process. The paste was then coating on the pretreated nickel foam, which was more stable than stainless steel and had a microporous structure to increase the contact area. Then the fashioned electrode was placed in the mold and pressed by a powder pressing machine at 15 Mpa for 30 min. After molding, the electrode was immersed in water at 60℃ for 3 h and in acetone at room temperature for 10 h. Finally, the electrode was calcined in a muffle furnace at 300℃ for 30 min with a heating rate of 3℃/min. To obtain GDE of different graphite-PTFE mass ratios, the addition amount of PTFE could be changed to 2.5 g (1:1), 1.25 g (1:2) and 0.625 g (1:4).

2.3. Structural characterization

The morphology of the samples was characterized by Field emission scanning electron microscopy (FE-SEM) (FE-SEM; Zeiss, Germany, ULTRA PLUS). The crystalline phases and crystallite size of the samples was characterized with X-ray diffractometry (XRD) (Bruker, Germany, AXS-8 Advance) at a scan rate of 5° min^{-1}. The BET surface area and the contact angle of the samples were characterized by Drop Shape Analyzer (KRUSS, Germany, DSA100).

2.4. Photoelectrochemical measurements

The photo response of theWO$_3$ NFA photoanode was carried out using a three-electrode system with the samples as the working electrode, platinum as the counter electrode and Ag/AgCl electrode as the reference electrode The working electrode potential and current were controlled by an electrochemical workstation (CHI 660c, CH Instruments Inc. USA). A 350 W Xe lamp was used as artificial light source, without further description, all experiments were carried out under visible light irradiation (light intensity, 100 mW cm^{-2}). The electrolyte was a 0.1 M Na_2SO_4 solution. The linear sweep voltammograms (LSV) were carried out under chopped light irradiation. The scan rate for the linear sweep voltammetry was 10 mV s^{-1}.

2.5. The self-driven PEC system for H_2S splitting

The self-driven PEC system for H_2S splitting was based on a custom-built double-chamber reactor with a proton membrane (Bofeilai Technology Co., Ltd.) and a corollary equipment for S collection. The self-bias photoanode and GDE cathode were put in the anodic and cathodic compartment, respectively. The electrolytes in the anodic and cathodic compartments were 100 mL 0.5 M H_2SO_4 containing 0.2 mol/L of KI and 100 mL 0.5 M H_2SO_4 respectively. Under illumination, H_2S was periodically pumped into the anodic compartment following a filtration through a corollary S collection device and the filtered solution was injected back to the anodic compartment. H_2O_2 was generated in the cathodic cell and the concentration was determined through potassium titanium oxalate spectrophotometry by a UV-VIS spectrophotometer (TU1810, Universal Analysis, Beijing, China) at its maximum absorption wavelength of 410 nm [30].

3. Results and discussion

3.1. Characterization of the electrodes

The top-view SEM image of the WO_3 NFA was shown in Fig. 1 (a). It can be seen that the WO_3 film had a plate-like morphology and the nanoplates adhered tightly and uniformly on the FTO substrate. The FTO substrate was totally covered by the WO_3 nanoplates without any empty region. The WO_3 nanoplates were directly grown on FTO in one step with no seed layer. This direct growth method could avoid the
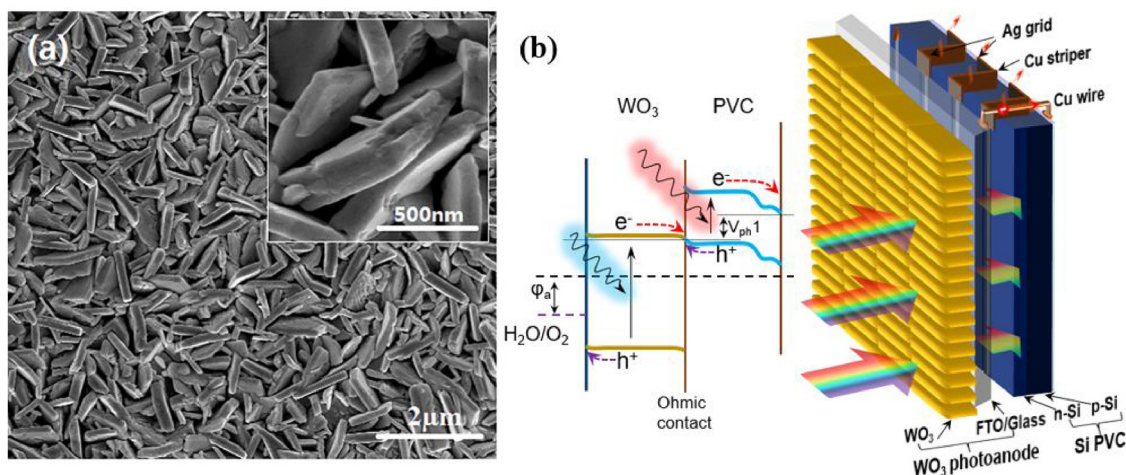
Fig. 1. (a) SEM image of the WO$_3$ NFA; (b) The schematic diagram of the self-bias photoanode of WO$_3$ NFA/SiPVC.

grain boundaries of the seed layer, which would reduce the resistance between the photocatalyst and the FTO substrate and thus improve the PEC performance. Previews research showed that the addition of a seed layer or a structure-directing agent resulted in an asymmetrical or discrete distribution of WO$_3$ NFA on the FTO [31–34]. Such an asymmetrical or discrete distribution of WO$_3$ NFA wasn't observed in our samples. As previously reported [35], the WO$_3$ NFA was of orthorhombic phase and the absorption edge lies at 450 nm (Figure S3). The prepared WO$_3$ NFA has good stability (Figure S4(a)) and photocatalytic capacity under solar light irradiation (Figure S4(b)). It also exhibited incident-photon-to-charge conversion efficiency (IPCE) behavior in the range of 350–470 nm (Figure S4(c)), which is roughly consistent with the light absorption spectrum of the WO$_3$ NPA. This means that the conversion of the absorbed photons into photocurrent occurred successfully in the photoanodes.

Fig. 1 (b) shows the schematic diagram of the self-bias photoanode with WO$_3$ NFA as the front photoanode material and a commercial Si cell as the rear photovoltaic cell. The particular structure of Si PVC was shown in Figure S1. The WO$_3$ and Si PVC are sealed together as a monolithic photoelectrode to simultaneously maximize light utilization and minimize complexity of device fabrication. The Si PVC was adhered to the back of theWO$_3$ NFA and sealed by silicone rubber. The front WO$_3$ NFA mainly absorbs short-wavelength part of sunlight and generates electron/hole pairs. The long-wavelength light irradiates though the WO$_3$ NFA and will be captured by the rear Si PVC to generate additional bias (Figure S5). The photogenerated holes of WO$_3$ NFA transfer to the electrode/electrolyte interface, meanwhile the electrons get accelerated via the rear Si PVC. Due to the bias by Si PVC, the WO$_3$ NFA/SiPVC photoanode could be self-sustaining in the PEC H$_2$S splitting.
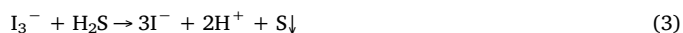
The schematic diagram of the GDE was shown in Fig. 2 (a). Two pieces of graphite and one piece of nickel foam sandwiched between them made up the H$_2$O$_2$-generating GDE. Fig. 2 (c) shows the SEM image of the nickel foam, which acts as the conducting material of the GDE. It can be observed that the nickel foam has highly-developed hole structure and large specific surface area, which will allow more molecular O$_2$ to contact the electrode. Besides, nickel was relatively stable. These qualities made nickel foam a better choice than stainless steel, which was used as the conducting material in previous research [36]. The surface SEM of GDE were shown in Fig. 2 (d). It can be observed that the surface of the electrode was loose and porous. With the BET surface area of 8.5766 m^2/g, the porous structure of GDE could benefit the delivery of O$_2$ and promote the generation of H$_2$O$_2$. The PTFE was added during the preparation of GDE to bond the graphite powder. After the electrode took shape, part of the PTFE would be leached by acetone, which could help to shape the porous structure of the

electrode. The surface of the GDE was strongly hydrophobic, with a contact angle of 115.0° (Fig. 2(b)), which could enhance the transfer of O$_2$ and increase the output of H$_2$O$_2$. The reaction pathway of oxygen reduction has been proved by LSV tests and Koutechy-Levich (K–L) calculation. As shown in Figure S4(d), the GDE cathode has excellent selectivity of two-electron reduction of molecular oxygen.

3.2. Photoelectrocatalytic splitting of H$_2$S

The WO$_3$/Si PVC photoanode and GDE cathode was applied in the PEC conversion of H$_2$S into elemental S and H$_2$O$_2$. As known, direct oxidation of S^{2-} using most semiconductor photoanode commonly leads to the formation of polysulfide (S$_x^{n-}$) by hydroxyl radical (E° = 3.2 V vs. NHE) or photoholes (E° = 2.81 V vs. NHE) because of their high oxidation potential [37], thus a typical yellow clarifying solution was only obtained (Figure S6). The polysulfide can be furtherly confirmed by a qualitative analysis of HCl, in which the milk white turbidity was observed after dilute HCl was added into the yellow clarifying solution. The results indicated that H$_2$S could be easily turned into polysulfide (S$_x^{n-}$). In this case, the promoter has to be introducd into the PEC system that makes the S^{2-} totally converted into S. I- ion is well-known hole trapping agent which can greatly enhance the separation of electron-hole pair and increase the photoconversion efficiency. In the PEC system [37,38], I- ions could be first oxidized into I$_3$- ions by WO$_3$ and thereafter H$_2$S could be oxidized into S by I$_3$- ions which was then reduced to I- again for the next cycle. Based on the principle, the device configuration and the operation mechanism of the PEC splitting H$_2$S system was shown in Fig. 3 (a) in which the WO$_3$/SiPVC photoanode and GDE cathode were placed in the anodic compartment and cathodic compartment respectively, separated by a PEM (Proton Exchange Membrane). During operation, H$_2$S was injected into the anodic compartment and elemental S was collected through an accessorial device. In the meantime, H$^+$ was transformed into H$_2$O$_2$ in the cathode region. The reactions (Eqs. (1)–(4) were shown as follows:

Anodic compartment:

$$WO_3 + h\nu \rightarrow e^- + h^+ \tag{1}$$

$$3I^- + 2h^+ \rightarrow I_3^- \tag{2}$$

$$I_3^- + H_2S \rightarrow 3I^- + 2H^+ + S\downarrow \tag{3}$$

Cathodic compartment:

$$2H^+ + O_2 + 2e^- \rightarrow H_2O_2 \tag{4}$$

Fig. 3b shows the open-circuit voltage (V$_{OC}$) of the PEC system under chopped illumination. As can be seen, the V$_{OC}$ values were − 0.22 V
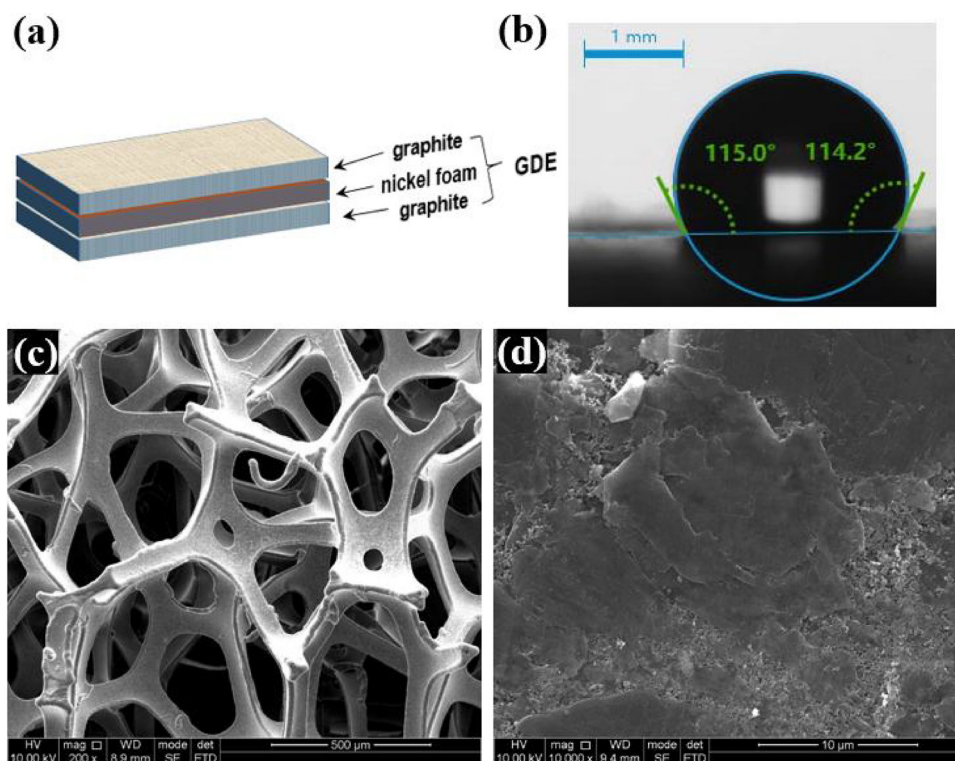
Fig. 2. (a) The schematic diagram of the GDE; (b) The contact angle of the GDE; (c) The SEM image of the nickel foam and (d) the surface of the GDE.

under dark and rose to 2.1 V under illumination. This is according with the photovoltage generated by the rear Si PVC (V ph = V $_{ph1}$ + V $_{ph2}$ + V $_{ph3}$ + V $_{ph4}$) (Figure S7). This result indicates that the PEC system can be driven by domestic bias.

The H_2S splitting was carried out under visible light illumination when H_2S was periodically pumped into the anodic compartment. Fig. 4 (a) shows the variation of photocurrent and the relevant color change of the solution in the whole process. In the initial phase, the photocurrent was about 14 mA and the solution color of the anodic compartment gradually changed from clear and colorless to canary yellow and to vivid red, which indicated the generation of I_3^-. After the injection of gas H_2S, the photocurrent suddenly fell to about 2 mA while the vivid red solution changed into a faint yellow turbidity simultaneously. This illustrated the formation of elemental S which was nearly insoluble in

water. A clear and colorless solution was achieved again after the turbidity was filtered out. Simultaneously, the photocurrent returned to 14 mA. This process could be constantly repeated in a long term and abundant elemental S would be collected. S production won't influence the performance of WO_3 and it can be reused (Figure S8). In the whole process, the photocurrent was kept at about 14 mA except when gas H_2S was injected into the anodic compartment. This process can be confirmed by investigating the ion ratio of I^-/I_3^- during the operation. It was found from Figure S9 that I^- ions gradually converted to I_3^- ions in the initial operation of 1000s. When H_2S was injected in the anodic compartment, I_3^- ions react with H_2S and was converted into I^- ions again and S was generated in the meantime. After that, the system entered a second cycle (Figure S9) and the concentrations of I^- and I_3^- exhibited a dynamic equilibrium. The production rate of S through the
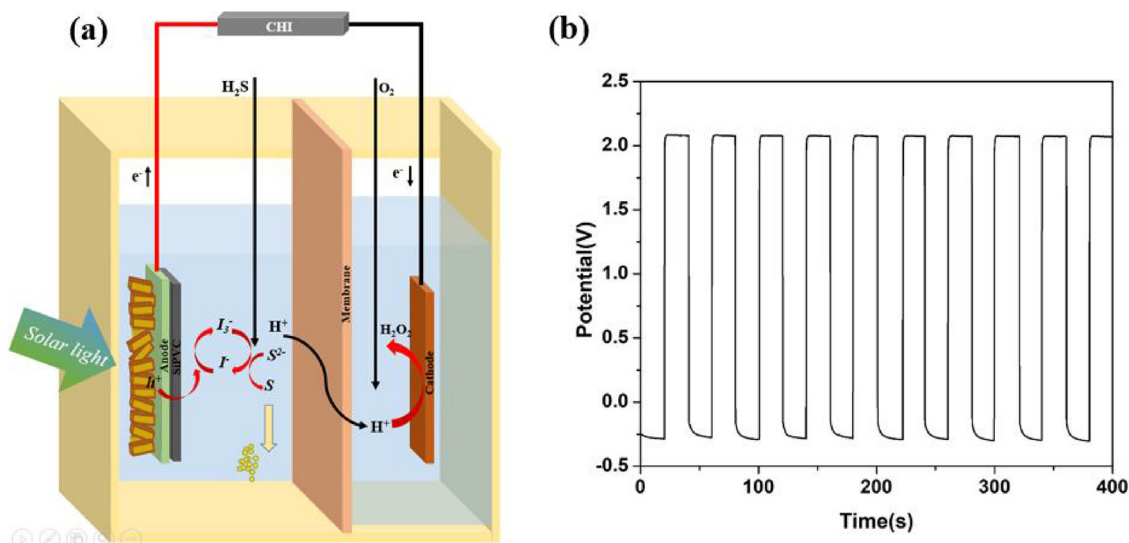

Fig. 3. (a) The schematic diagram of the PEC system; (b) V_{OC} of the PEC-H_2S system.
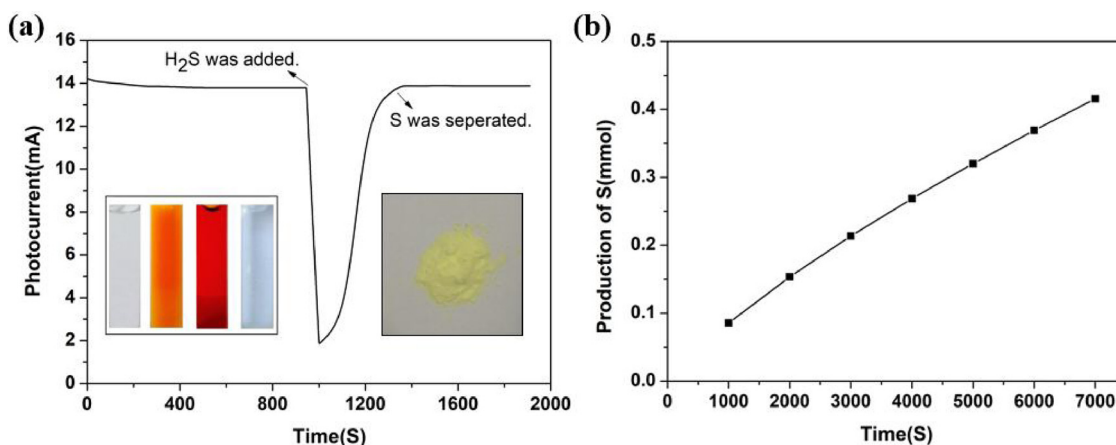
Fig. 4. (a) The current and solution color changes before and after the injection of H_2S; (b) The S recovery during a long-term operation.
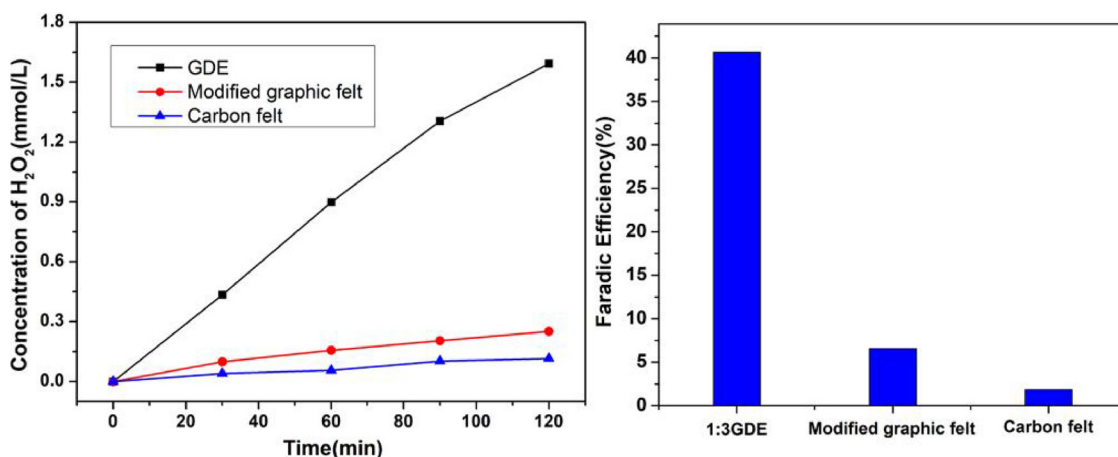

Fig. 5. (a) Production of H_2O_2 and (b) Faradic efficiency by different cathodes in the PEC system.
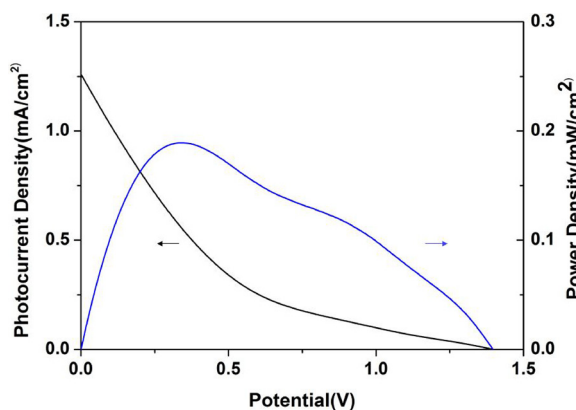

Fig. 6. I–V characteristic curve and power density curve of the PEC-H_2S system.

PEC system was shown in Fig. 4(b). It can be seen that the production rate of S was maintained at about 6.816 mg h^{-1}, respectively, and no polysulfide appeared, suggesting that the S^{2-} was totally converted into S.

3.3. H_2O_2 production

Fig. 5 (a) shows the concentrations of H_2O_2 generated by different photocathodes. The highest rate of 0.80 mmol/L/h was obtained by GDE cathode, which is 6 and 13 times larger than those of modified graphic felt and normal carbon felt cathode respectively. This contributes to the distinctive structure of the GDE as previously mentioned. In previous research, H_2O_2 was generated through an anthraquinone (AQ) process. The hydrogenation of AQ with H_2 produces anthrahydroquinone (H_2AQ) and subsequent oxidation of H_2AQ by O_2 produces H_2O_2 [21]. AQ process was far more complicated and energy-consuming. On contrast, our process just needed aeration and no medicine was added [18]. The Faradic efficiency was also calculated according to the following formula:

Table 1
The production of S and H_2O_2 and electricity generation during the first three cycles.

Cycle	1		2		3	
Time(S)	0–1000	1000–2000	2000–3000	3000–4000	4000–5000	5000–6000
S(mmol)	0.086	0.154	0.214	0.269	0.320	0.369
H_2O_2(mmol)	0.023	0.046	0.070	0.093	0.116	0.139
Electricity generation(mWh)	0.317	0.633	0.950	1.27	1.58	1.90

$$FE = \frac{nFc_{H_2O_2}V}{\int_0^t Idt} \times 100\%$$

The n represents the electron transfer number. F represents Faraday constant. $c_{H_2O_2}$ represents the concentration of H_2O_2. V represents the volume of the solution. As shown in Fig. 5 (b), the Faradic efficiency of GDE was 40.7%, which was 21 and 67 times higher than those of carbon felt and Pt cathode respectively.

The PTFE: graphite mass ratio PTFE is crucial to the performance of the GDE cathode. PTFE serves two purposes: One is bonding the graphite and other materials to form a tough electrode. The other is strengthening the hydrophobicity property of the electrode. However, overmuch PTFE will reduce the porosity of the GDE and influence the O_2 transfer. Besides, it is an insulating material so excess PTFE will increase the electrode's resistance and degrade its electrochemical performance. Therefore, an optimal addition amount of PTFE should be determined. In this study, the best GDE was made by the PTFE: graphite mass ratio of 1:3 (Figure S10).

3.4. Electricity generation

As shown in Fig. 6, the electricity generation during the process was studied by assessing the output power density. The decomposition of H_2S into S and H_2O_2 was an exothermic process, in which the reactions are beneficial to the electricity generation by the photoanode. First, photogenerated electrons and holes were generated under illumination in the anodic compartment. I^- could rapidly trap the photogenerated holes and the photogenerated electrons were delivered to the cathodic compartment. This process highly promoted the charge separation efficiency. On the other hand, the rear PVC could capture the filtered long-wavelength light which improved the light utilization and mainly contributed the electricity generation. As shown in Fig. 6, the system's maximum power density was about 0.19 mW/cm².

To assess the performance of the PEC system, the yields of S and H_2O_2 were continuously recorded within a long-term operation. Table 1 shows the yields of S and H_2O_2 and electricity generation within three cycles. The production rates of S and H_2O_2 were 0.60 mmol/h and 0.08 mmol/h, respectively, and electricity generation rate was about 0.19 mW/cm². The deficiency of H_2O_2 may result from the reduction of O_2 into H_2O. The results also suggested that H_2S was entirely converted into S and no polysulfide was generated.

4. Conclusions

In summary, we proposed a self-driven PEC system, with WO_3/SiPVC as photoanode and GDE as cathode, to convert H_2S into S and H_2O_2, and electricity was generated simultaneously. The performance of the self-driven PEC system was studied by measuring the photoelectric effect and the production of S and H_2O_2. The results demonstrated that the production rate of S was maintained at about 6.816 mg h⁻¹ and no polysulfide appeared. The concentration of H_2O_2 was much higher than previous research's, with an output of 0.8 mmol/L/h. The system's maximum power density was about 0.19 mW/cm². We hope that the novel PEC system gives its promising in efficient and sustainable way of H_2S waste recycling and energy recovery.

Acknowledgement

Appendix A. Supplementary data

Supplementary material related to this article can be found, in the online version, at doi:https://doi.org/10.1016/j.apcatb.2018.07.051.

References

[1] T. Nunnally, K. Gutsol, A. Rabinovich, A. Fridman, A. Starikovsky, A. Gutsol, R.W. Potter, Dissociation of H_2S in non-equilibrium gliding arc "tornado" discharge, Int. J. Hydrogen Energy 34 (18) (2009) 7618–7625.

[2] K.A. Rabbani, W. Charles, A. Kayaalp, R. Cord-Ruwisch, G. Ho, Pilot-scale biofilter for the simultaneous removal of hydrogen sulphide and ammonia at a wastewater treatment plant, Biochem. Eng. J. 107 (2016) 1–10.

[3] A.T. Angela, R. Didier, K. Nicolas, K. Valérie, A parametric study of the UV-a photocatalytic oxidation of H_2S over TiO_2, Appl. Catal. B: Environ. 115 (2012) 209–218.

[4] A. PiEPlu, O. Saur, J.C. Lavalley, O. Legendre, C. NEDez, Claus catalysis and H_2S selective oxidation, Catal. Rev.: Sci. Eng. 40 (4) (1998) 409–450.

[5] S. Song, Z. Liu, Z. He, A. Zhang, J. Chen, Impacts of morphology and crystallite phases of titanium oxide on the catalytic ozonation of phenol, Environ. Sci. Technol. 44 (10) (2010) 3913.

[6] L. Jing, H. Fu, B. Wang, D. Wang, B. Xin, Effects of Sn dopant on the photoinduced charge property and photocatalytic activity of TiO_2 nanoparticles, Appl. Catal. B: Environ. 62 (2016) 282–291.

[7] L. Zheng, X. Yu, M. Long, Q. Li, Humic acid mediated visible light degradation of phenol on the phosphate and Nafion modified TiO2 surface, Chin. J. Catal. 38 (12) (2017) 2076–2084.

[8] X. Li, S. Liu, D. Cao, R. Mao, X. Zhao, Synergetic activation of H_2O_2 by photo-generated electrons and cathodic Fenton reaction for enhanced self-driven photo-electrocatalytic degradation of organic pollutants, Appl. Catal. B:Environ. 235 (2018) 1–8.

[9] M. Long, L. Zheng, Engineering vacancies for solar photocatalytic applications Chinese Journal of Catalysis 38 (4) (2017) 617–624.

[10] L. Xia, J. Li, J. Bai, L. Li, S. Chen, B. Zhou, Preparation of $BiVO_4$ photoanode with exposed (040) facets for enhanced photoelectrochemical performance, Nano-Micro Letters (11) (2018) 10.

[11] X. Li, J. Li, J. Bai, Y. Dong, L. Li, B. Zhou, The inhibition effect of tert-butyl alcohol on the TiO_2 nano assays photoelectrocatalytic degradation of different organics and its mechanism, Nano-Micro Letters 8 (3) (2016) 221–231.

[12] R. Wang, J. Bai, Y. Li, Q. Zeng, J. Li, B. Zhou, $BiVO_4/TiO_2(N_2)$ nanotubes hetero-junction photoanode for highly efficient photoelectrocatalytic applications, Nano-Micro Lett. 9 (14) (2017).

[13] Y. Dong, J. Li, X. Li, B. Zhou, The promotion effect of low-molecular hydroxyl compounds on the nano-photoelectrocatalytic degradation of fulvic acid and mechanism, Nano-Micro Lett. 5 (4) (2016) 320–327.

[14] A.P. Bhirud, S.D. Sathaye, R.P. Waichal, J.D. Ambekar, C.J. Park, B. Kale, In-situ preparation of N-TiO2/graphene nanocomposite and its enhanced photocatalytic hydrogen production by H_2S splitting under solar light, Nanoscale 7 (11) (2015) 5023–5034.

[15] M.S. Selvan, M.D. Mckinley, J.L. Atwood, Liquid−liquid equilibria for toluene + heptane + 1-ethyl-3-methylimidazolium triiodide and toluene + heptane + 1-butyl-3-methylimidazolium triiodide, J. Chem. Eng. Data 45 (5) (2000) 841–845.

[16] A.S.P. Gomes, L. Visscher, H. Bolvin, T. Saue, S. Knecht, T. Fleig, E. Eliav, The electronic structure of the triiodide ion from relativistic correlated calculations: a comparison of different methodologies, J. Chem. Phys. 133 (6) (2010) 272.

[17] T. Luo, J. Bai, J.H. Li, Q. Zeng, Y. Ji, L. Qiao, Xiaoyan Li, Baoxue Zhou, Self-driven photoelectrochemical splitting of H_2S for S and H_2 recovery and simultaneous electricity generation, Environ. Sci. Technol. 51 (2017) 12965–12971.

[18] Xu Zong, Hongjun Chen, Brian Seger, Thomas Pedersen, Matthew S. Dargusch, Eric W. McFarland, Can Li, Lianzhou Wang, Selective production of hydrogen peroxide and oxidation of hydrogen sulfide in an unbiased solar photoelectrochemical cell, Energy Environ. Sci. 7 (2014) 3347.

[19] J.K. Edwards, B. Solsona, E.N. Ntainjua, A.F. Carley, A.A. Herzing, C.J. Kiely, G.J. Hutchings, ChemInform abstract: switching off hydrogen peroxide hydro-genation in the direct synthesis process, Science 323 (2009) 1037–1041.

[20] J.H. Lunsford, The direct formation of H_2O_2 from H_2 and O_2 over palladium cata-lysts, Catal. 216 (2003) 455–460.

[21] J.M. Campos-Martin, G. Blanco-Brieva, J.L.G. Fierro, Hydrogen peroxide synthesis: an outlook beyond the anthraquinone process, Angew. Chem., Int. Ed. 45 (2006) 6962–6984.

[22] Q.P. Chen, J.H. Li, B.X. Zhou, M.C. Long, H.C. Chen, Y.B. Liu, W.M. Cai. Preparation of well-aligned WO_3 nanoflake arrays vertically grown on tungsten substrate as photoanode for photoelectrochemical water splitting, Electrochem. Commun. (2012) 153–156.

[23] J.F. Carneiro, R.S. Rocha, P. Hammer, R. Bertazzoli, M.R.V. Lanza, Hydrogen per-oxide electrogeneration in gas diffusion electrode nanostructured with Ta_2O_5, Appl. Catal., A 517 (2016) 161–167.

[24] M.H.M.T. Assumpcão, R.F.B. De Souza, D.C. Rascio, J.C.M. Silva, M.L. Calegaro, I. Gaubeur, Electrogeneration of hydrogen peroxide in gas diffusion electrodes modified with tert-butyl-anthraquinone on carbon black support, Carbon 61 (5) (2013) 236–244.

[25] R. Beranek, (Photo)electrochemical methods for the determination of the band edge positions of TiO2-based nanomaterials, Adv. in Phys. Chem. 2011 (1687-7985) (2016) 1–2.

[26] D. Wang, Y. Li, G. Li Puma, C. Wang, P. Wang, W. Zhang, Q. Wang, Dye-sensitized photoelectrochemical cell on plasmonic Ag/AgCl @ chiral TiO_2 nanofibers for treatment of urban wastewater effluents, with simultaneous production of hydrogen and electricity, Appl. Catal. B: Environ. 168–169 (2015) 25–32.

[27] Q.P. Chen, J.H. Li, X.J. Li, K. Huang, B.X. Zhou, W.M. Cai, W.F. Shangguan, Visible-light responsive photocatalytic fuel cell based on WO_3/W photoanode and Cu_2O/Cu

photocathode for simultaneous wastewater treatment and electricity generation, Environ. Sci. Technol. 46 (2012) 11451–11458.

[28] R. Solarska, R. Jurczakowski, J. Augustynski, A highly stable,efficient visible-light driven water photoelectrolysis system using a nanocrystalline WO 3 photoanode and a methane sulfonic acid electrolyte, Nanoscale 4 (5) (2012) 1553.

[29] M.S. Prévot, K. Sivula, Photoelectrochemical tandem cells for solar water splitting, J. Phys. Chem. C 117 (35) (2013) 17879–17893.

[30] Y. Zhang, M. Gao, X. Wang, S. Wang, R. Liu, Enhancement of oxygen diffusion process on a rotating disk electrode for the electro-fenton degradation of tetracycline, Electrochim. Acta 182 (2015) 73–80.

[31] E.L. Miller, Solar Hydrogen Production by Photoelectrochemical Water Splitting: The Promise and Challenge, (2010).

[32] S.S. Kalanur, Y.J. Hwang, S.Y. Chae, O.S. Joo, Facile growth of aligned WO$_3$ nanorods on FTO substrate for enhanced photoanodic water oxidation activity, J. Mater. Chem. A 1 (2013) 3479.

[33] J. Su, X. Feng, J.D. Sloppy, L. Guo, C.A. Grimes, Vertically aligned wo$_3$ nanowire arrays grown directly on transparent conducting oxide coated glass: synthesis and photoelectrochemical properties, Nano Lett. 11 (2011) 203–208.

[34] J. Su, L. Guo, N. Bao, C.A. Grimes, Nanostructured WO$_3$/BiVO$_4$ heterojunction films for efficient photoelectrochemical water splitting, Nano Lett. 11 (2011) 1928–1933.

[35] Q. Zeng, J. Li, J. Bai, X. Li, L. Xia, B. Zhou, Preparation of vertically aligned WO$_3$ nanoplate array films based on peroxotungstate reduction reaction and their excellent photoelectrocatalytic performance, Appl. Catal., B :Environ 202 (2017) 388–396.

[36] Q. Yu, M. Zhou, L. Lei, Novel gas diffsion electrode system for effective production of hydrogen peroxide, Acta Phys.- Chem. Sin. 22 (7) (2006) 883–887.

[37] R.W. Matthews, Chem Inform Abstract, Photocatalytic oxidation of organic contaminants in water: an aid to environmental preservation, Cheminform 64 (9) (2009) 1285–1290.

[38] H. Zhu, A.A. Hagfeldt, G. Boschloo, Photoelectrochemistry of mesoporous NiO electrodes in Iodide/Triiodide electrolytes, J. Phys. Chem. C 111 (47) (2007) 17455–17458.